IEEE Access
Multidisciplinary | Rapid Review | Open Access Journal

Received September 26, 2019, accepted October 19, 2019, date of publication October 23, 2019, date of current version November 7, 2019.

Digital Object Identifier 10.1109/ACCESS.2019.2949061

A Novel RFDI-FTC System for Thrust-Vectoring Aircraft Undergoing Control Surface Damage and Actuator Faults During Supermaneuverable Flight

XIAOSHAN MA[1], WENHAN DONG[2], AND BINGQIAN LI[3]
[1]Graduate College, Air Force Engineering University, Xi'an 710038, China
[2]Aviation Maintenance NCO Academy, Air Force Engineering University, Xinyang 464000, China
[3]Aeronautics Engineering College, Air Force Engineering University, Xi'an 710038, China

Corresponding author: Xiaoshan Ma (maxiaoshan@buaa.edu.cn)

ABSTRACT In this paper, a novel robust fault detection and identification and fault-tolerant control (RFDI-FTC) system is proposed for thrust-vectoring aircraft (TVA) during supermaneuverable flight. To this end, a TVA model that incorporates control surface damage, actuator faults, disturbances, and aerodynamic parameter uncertainty is described, and a novel RFDI-FTC system is designed for the TVA model, which includes 1) an RFDI subsystem with robustness to disturbances and parameter uncertainty and sensitivity to control surface damage and actuator faults by multiple adaptive observers; 2) a command filter FTC subsystem to eliminate the differential expansion in traditional backstepping control and to compensate for control surface damage, actuator faults, disturbances and parameter uncertainty; and 3) a stability analysis for the RFDI-FTC system. The simulation results are given to demonstrate the effectiveness and potential of this system.

INDEX TERMS RFDI-FTC system, TVA, control surface damage, actuator fault, robust FDI, adaptive observer, command filter FTC.

I. INTRODUCTION

Thrust-vectoring technology [1]–[3] is one of the most significant methodologies to control an aircraft's roll, pitch, and yaw maneuvering at a low airspeed and a high attack angle, called supermaneuverable flight [4], [5], which can realize control surface and actuator redundancy and improve flight performance by coordinating thrust-vectoring paddle deflection. In close air combat, thrust-vectoring aircraft (TVA) can change the pointing direction quickly to respond to various battlefield situations by supermaneuverable flight [6], [7]. The strong nonlinear behavior and aerodynamic force coupling [8], [9] produced by supermaneuverable flight increases the probability of control surface damage and actuator faults, seriously endangering flight safety. On the other hand, lateral and longitudinal thrust vectoring can compensate for control surface damage and actuator faults in the rudder and elevator, respectively, which can improve the fault tolerance performance. Therefore, a robust fault detection and identification and fault-tolerant control (RFDI- FTC) system for TVA during supermaneuverable flight has great significance for air combat.

Fault detection and identification are necessary for fault-tolerant control, and some progress has been made in the fault detection and identification (FDI) field. The problems of residual-based actuator fault detection are investigated in a previous work [10] for a class of uncertain linear systems with disturbances, where the interval observer is robust to disturbances but sensitive to actuator faults in the sense of interval estimation. Reference [11] introduces a model-based FDI technique for the diagnosis of machine health conditions, which detects and identifies faults by extracting fault signal information based on a defined relationship between fault signals and observers. The disturbances and uncertainties are ignored in that paper. A novel online fault detection and identification strategy for a class of continuous piecewise affine systems is established in a previous work [12], whose main contributions with respect to the state of the art are the recursive nature of the proposed scheme and the consideration of parametric uncertainties in both partitions and in

The associate editor coordinating the review of this manuscript and approving it for publication was Zhongyang Fei.

subsystem parameters. A navigation system fault detection model is established based on belief rules in a previous work [13], where the system-measured residuals and change rates are used as the inputs of a belief rule model and a parameter recursive estimation algorithm is presented for the online detection model. Because this method neglects the influence of disturbances and uncertainty, some false alarms may occur. Reference [14] investigates the active fault-tolerant control problem for the attitude system of a rigid satellite with parameter uncertainty, unknown exogenous disturbances and actuator time-varying faults. Han, Y. et al. proposed a fault detection algorithm for an actuator stuck fault of an aircraft with multiple control surfaces [15], which is composed of an adaptive observer to detect faults and a bias estimation algorithm to estimate the stuck position. As with most of the literature mentioned above, disturbances and uncertainties, which were not taken into consideration, may cause false alarms. Reference [16] designs a fault detection observer for linear time invariant systems with unknown disturbances, where the sufficient conditions for the existence of the fault detection observer narrow the application scope. Denis, V. E. et al. proposed a hybrid monitoring scheme with high robustness and performance for an electrical flight control system [17], where a robust finite-time differentiator is used to estimate derivatives in a noisy environment. This method is superior to the traditional fault detection method because of the robustness to disturbances, but the parameter uncertainty is not taken into consideration. The above analyses show that most of the literature does not consider disturbances or parameter uncertainty in the FDI design process, which may cause a high false alarm rate because strong disturbances and parameter perturbation frequently occur during supermaneuverable flight. Therefore, novel RFDI is necessary for TVA to maintain robustness to disturbances and parameter uncertainty and sensitivity to control surface damage and actuator faults.

Control surface damage and actuator faults [18] seriously endanger flight safety and present a major challenge in completing the scheduled task, necessitating fault-tolerant control to address these issues. Salman, I. et al. proposed an active fault-tolerant control scheme for a relatively electric-based aircraft equipped with a dissimilar redundant actuator system [19], where the control allocation scheme together with an integral sliding-mode controller is retrofitted with the state feedback control law and engages the redundant actuators into the loop. An active fault-tolerant control strategy was designed for an aircraft with a dissimilar redundant actuation system under vertical tail damage in a previous work [20], where a composite method of model reference adaptive control integrating a linear quadratic regulator was proposed to reconfigure the fault-tolerant control law. Rajamani, D. et al. proposed a robust fault-tolerant control scheme using an accurate emulator-based identification technique for aircraft flight systems [21], and a robust Kalman filter-based state feedback controller was designed to compensate the system faults. Shen, Q. K. et al. proposed a novel fault diagnosis algorithm by using the backstepping approach [22], which removes the classical assumption that the time derivative of output error should be known, and an observer-based FTC scheme was proposed for a class of uncertain nonlinear systems with actuator faults that guarantees that all signals of the closed-loop system are ultimately semiglobally uniformly bounded and converge to a small neighborhood around the origin by appropriate choice of designed parameters. The existence condition of the FDI observer must be satisfied. A supervisory adaptive fault-tolerant control scheme was proposed in a previous work [23] for a class of uncertain nonlinear systems with multiple inputs, which consists of (1) an adaptive compensation mode to compensate for the failure of an actuator group as long as at least one actuator of the group works normally and (2) a switching mode to switch the controller from a failed group to a healthy one when a fault is detected by one of the monitoring functions that are constructed to supervise variables related to system stability. A robust fault-tolerant control scheme was proposed in a previous work [24] for uncertain nonlinear systems with actuator faults and lock-in-place and float faults, which consists of an adaptive second-order sliding-mode strategy and a backstepping procedure. Lamouchi, R. et al. addressed the problem of passive fault-tolerant control for linear parameter-varying systems subject to actuator faults [25], and FTC based on linear state feedback was designed to compensate for the impact of actuator faults on the system performance by stabilizing the closed-loop system using interval observers, designed based on the discrete-time Luenberger observer structure. The above analyses show that most of the literature does not consider control surface damage together with actuator faults, nor does it consider disturbances and parameter uncertainties in the FTC design process. These factors should be addressed together to ensure safety and stability during supermaneuverable flight. To this end, FTC based on the RFDI results, backstepping control and command filter technology is proposed in this paper.

The novel contributions of this paper are as follows. First, this paper comprehensively investigates an RFDI-FTC system for TVA with control surface damage, actuator faults, disturbances and parameter uncertainty in conjunction with highly unsteady and nonlinear flows during supermaneuverable flight. Moreover, the simulation results demonstrate thrust vector compensation for the aerodynamic control surface. Second, this paper proposes an RFDI mechanism for TVA to detect, identify and estimate control surface damage and evaluate actuator loss of effectiveness (LOE) faults and actuator stuck faults step by step and accurately; the whole RFDI mechanism can maintain robustness to disturbances and parameter uncertainties and sensitivity to control surface damage and actuator faults to reduce false alarms and increase the accuracy of FDI. Third, a novel command filter FTC system based on backstepping is proposed in this paper to eliminate the impact of differential expansion in traditional backstepping control, and the stability and effectiveness

are verified by Lyapunov function analysis and simulation, respectively.

This paper is organized as follows. In Section II, the TVA model with uncertain parameters, disturbances, control surface damage and actuator faults is presented. In Section III, an RFDI-FTC system is designed to achieve fault detection, identification and tolerance control, comprising three aspects: an RFDI mechanism based on multiple adaptive observers is proposed to detect and identify control surface damage and actuator faults under disturbances and parameter uncertainty; a command filter FTC system is designed to compensate for control surface damage, actuator faults, disturbances, and parameter uncertainty by combining backstepping control with fault parameters and command filter technology; and a stability analysis for the RFDI-FTC system is given. In Section IV, the simulation results are presented to illustrate the effectiveness of the proposed RFDI-FTC system, with concluding remarks in Section V.

II. PRELIMINARIES

The TVA model that incorporates control surface damage, actuator faults, disturbances and parameter uncertainty is described in this section.

A. TVA MODEL DESCRIPTION

The TVA model, built in a former study [1], can be divided into attitude-angle-loop and angle-velocity-loop components according to singular perturbation theory. The attitude-angle-loop component consists of $[\alpha\ \beta\ \mu]$, corresponding to the attack angle, side-slip angle, and bank angle, respectively, and the angle-velocity-loop component consists of $[p\ q\ r]$, corresponding to the spin, pitch, and yaw rates, respectively. The equations for the attitude-angle-loop and the angle-velocity-loop components can be described as:

$$\begin{cases} \dot{\boldsymbol{\psi}} = F(\boldsymbol{\psi}) + \boldsymbol{g}(\boldsymbol{\psi})\,\boldsymbol{\omega} \\ \dot{\boldsymbol{\omega}} = F(\boldsymbol{\omega}) + \boldsymbol{g}(\boldsymbol{\omega})\,\boldsymbol{u}, \end{cases} \tag{1}$$

where $\boldsymbol{\psi} = [\alpha\ \beta\ \mu]^{\mathrm{T}}$; $\boldsymbol{\omega} = [p\ q\ r]^{\mathrm{T}}$; $\boldsymbol{F}(\boldsymbol{\psi})$ and $\boldsymbol{F}(\boldsymbol{\omega})$ characterize the equation's nonlinearity;$\boldsymbol{g}(\boldsymbol{\psi})$ is a coefficient matrix; $\boldsymbol{g}(\boldsymbol{\omega})$ is the maneuvering moment matrix; and $\boldsymbol{u} = [\delta_a\ \delta_e\ \delta_r\ \delta_y\ \delta_z]^{\mathrm{T}}$ is the actual control signal for the angle-velocity-loop component, corresponding to the aileron deflection, elevator deflection, rudder deflection, and lateral and longitudinal thrust-vectoring paddle deflections. During supermaneuverable flight, highly unsteady and nonlinear flows cause aerodynamic parameter uncertainty and an unknown disturbance $\boldsymbol{d}$. Considering these factors, equation (1) can be described as:

$$\begin{cases} \dot{\boldsymbol{\psi}} = \boldsymbol{f}(\boldsymbol{\psi}) + \boldsymbol{A}(\boldsymbol{\psi})\,\boldsymbol{\eta}_{\boldsymbol{\psi}} + \boldsymbol{g}(\boldsymbol{\psi})\,\boldsymbol{\omega} \\ \dot{\boldsymbol{\omega}} = \boldsymbol{f}(\boldsymbol{\omega}) + \boldsymbol{B}(\boldsymbol{\omega})\,\boldsymbol{\eta}_{\boldsymbol{\omega}} + \boldsymbol{g}(\boldsymbol{\omega})\,\boldsymbol{u} + \boldsymbol{d}, \end{cases} \tag{2}$$

where $\boldsymbol{\eta}_{\boldsymbol{\psi}} \in \mathrm{R}^3$ are the uncertain aerodynamic parameters and $\boldsymbol{\eta}_{\boldsymbol{\omega}} \in \mathrm{R}^{12}$ are the uncertain aerodynamic-moment parameters. $\boldsymbol{A}(\boldsymbol{\psi})$ and $\boldsymbol{B}(\boldsymbol{\omega})$ are the coefficient matrixes for the uncertain parameters, and $\boldsymbol{f}(\boldsymbol{\psi})$ and $\boldsymbol{f}(\boldsymbol{\omega})$ characterize the nonlinearity.

B. CONTROL SURFACE DAMAGE MODELING

Control surface damage, which weakens the original aerodynamic effect [26], can be described as

$$\delta_i^R = r_i\delta_i, \quad r_i \in (0, 1], \tag{3}$$

where δ_i^R is the actual control signal sent from the ith control surface; δ_i is the input command, i.e., the control signal sent from the ith actuator; $r_i \in (0, 1]$ is the so-called damage parameter, and $r_i \in (0, 1)$ denotes that the ith control surface is damaged to a certain extent, with $r_i = 1$ denoting that the ith control surface is damage-free.

Hence, the TVA model with control surface damage can be described as

$$\begin{cases} \dot{\boldsymbol{\psi}} = \boldsymbol{f}(\boldsymbol{\psi}) + \boldsymbol{A}(\boldsymbol{\psi})\,\boldsymbol{\eta}_{\boldsymbol{\psi}} + \boldsymbol{g}(\boldsymbol{\psi})\,\boldsymbol{\omega} \\ \dot{\boldsymbol{\omega}} = \boldsymbol{f}(\boldsymbol{\omega}) + \boldsymbol{B}(\boldsymbol{\omega})\,\boldsymbol{\eta}_{\boldsymbol{\omega}} + \boldsymbol{g}(\boldsymbol{\omega})\,\boldsymbol{R}\boldsymbol{u} + \boldsymbol{d}, \end{cases} \tag{4}$$

where $\boldsymbol{R} = \mathrm{diag}\left[r_a, r_e, r_r, r_y, r_z\right]$.

C. ACTUATOR FAULT MODELING

In an actual flight control system, typical actuator faults [27] include the following four types: (1) stuck, (2) hard-over failure (HOF), (3) float, and (4) LOE. HOF is equivalent to being stuck at a max-min deflection position, and float is equivalent to being stuck at 0 rad. Therefore, stuck, HOF, and float for an actuator fault can be regarded as the same action [28], referred to as a stuck condition. Then, the actuator fault model can be designed as:

$$\delta_i = \sigma_i k_i \delta_{ci} + (1 - \sigma_i)\, k_i \delta_i, \tag{5}$$

where δ_{ci} is the ith actuator input command; $\sigma_i \in \{0, 1\}$ is the stuck fault parameter of the ith actuator, where $\sigma_i = 0$ indicates that the actuator is stuck and $\sigma_i = 1$ indicates that it is stuck-fault-free; $k_i \in (0, 1]$ is the LOE fault parameter of the ith actuator, where $k_i = 1$ denotes that the actuator is LOE-fault-free and $k_i \in (0, 1)$ indicates that it is undergoing an LOE fault to a certain extent; and $i = a, e, r, y, z$ denote the aileron, elevator, rudder, lateral and longitudinal thrust-vectoring paddle, respectively. Furthermore, we have

$$\boldsymbol{u} = \boldsymbol{\Sigma}\boldsymbol{K}\boldsymbol{u}_c + (\boldsymbol{I} - \boldsymbol{\Sigma})\,\boldsymbol{K}\boldsymbol{u}, \tag{6}$$

where $\boldsymbol{\Sigma} = \mathrm{diag}[\sigma_a, \sigma_e, \sigma_r, \sigma_y, \sigma_z]$, $\boldsymbol{K} = \mathrm{diag}[k_a, k_e, k_r, k_y, k_z]$ and $\boldsymbol{u}_c = [\delta_{ca}\delta_{ce}\delta_{cr}\delta_{cy}\delta_{cz}]^{\mathrm{T}}$.

Hence, system (4) with actuator fault model (6) can be transformed into

$$\begin{cases} \dot{\boldsymbol{\psi}} = \boldsymbol{f}(\boldsymbol{\psi}) + \boldsymbol{A}(\boldsymbol{\psi})\,\boldsymbol{\eta}_{\boldsymbol{\psi}} + \boldsymbol{g}(\boldsymbol{\psi})\,\boldsymbol{\omega} \\ \dot{\boldsymbol{\omega}} = \boldsymbol{f}(\boldsymbol{\omega}) + \boldsymbol{B}(\boldsymbol{\omega})\,\boldsymbol{\eta}_{\boldsymbol{\omega}} + \boldsymbol{g}(\boldsymbol{\omega})\,\boldsymbol{R}\boldsymbol{\Sigma}\boldsymbol{K}\boldsymbol{u}_c \\ \qquad + \boldsymbol{g}(\boldsymbol{\omega})\,\boldsymbol{R}(\boldsymbol{I} - \boldsymbol{\Sigma})\,\boldsymbol{K}\boldsymbol{u} + \boldsymbol{d}, \end{cases} \tag{7}$$

III. RFDI-FTC SYSTEM DESIGN

In this section, the RFDI-FTC system is designed for a TVA during supermaneuverable flight, which includes (1) an RFDI subsystem to detect and identify control surface damage and actuator faults under the influence of disturbances and parameter uncertainty and (2) a command filter FTC subsystem to compensate for control surface damage, actuator faults, disturbances and parameter uncertainty.

A. RFDI MECHANISM DESIGN

An RFDI mechanism is designed so that it is robust to disturbances and parameter uncertainty and sensitive to control surface damage and actuator faults. The mechanism consists of a fault detection observer to detect the TVA faults, a fault identification observer to identify the control surface damage and actuator faults and two actuator fault identification observers for the ith actuator to identify actuator fault types.

1) FAULT DETECTION

For the angle-velocity-loop component in equation (2), we design a cascade observer as follows:

$$\dot{\hat{\boldsymbol{\omega}}}_1 = \boldsymbol{L}_1\tilde{\boldsymbol{\omega}}_1 + \boldsymbol{f}(\boldsymbol{\omega}) + \boldsymbol{B}(\boldsymbol{\omega})\hat{\boldsymbol{\eta}}_{1\boldsymbol{\omega}} + \boldsymbol{g}(\boldsymbol{\omega})\boldsymbol{u} + \hat{\boldsymbol{d}}, \tag{8}$$

where $\hat{\boldsymbol{\omega}}_1$ is the estimation value of $\boldsymbol{\omega}$ and $\tilde{\boldsymbol{\omega}}_1 = \hat{\boldsymbol{\omega}}_1 - \boldsymbol{\omega}$ is the estimation error; $\boldsymbol{L}_1$ is a solution to the Lyapunov matrix equation $\boldsymbol{L}_1^{\mathrm{T}}\boldsymbol{P}_1 + \boldsymbol{P}_1\boldsymbol{L}_1 = -\boldsymbol{Q}_1$ with $\boldsymbol{P}_1 = \boldsymbol{P}_1^{\mathrm{T}} > 0$ and $\boldsymbol{Q}_1 = \boldsymbol{Q}_1^{\mathrm{T}} > 0$; and $\hat{\boldsymbol{\eta}}_{1\boldsymbol{\omega}}$ is designed as follows to compensate for the parameter uncertainty.

$$\dot{\hat{\boldsymbol{\eta}}}_{1\boldsymbol{\omega}} = \mathrm{Proj}_{\hat{\boldsymbol{\eta}}_{1\boldsymbol{\omega}}}\left\{\boldsymbol{\Gamma}_1\left[-\boldsymbol{B}^{\mathrm{T}}(\boldsymbol{\omega})\boldsymbol{P}_1\tilde{\boldsymbol{\omega}}_1\right]\right\}, \tag{9}$$

where $\boldsymbol{\Gamma}_1$ is a positive matrix and $\mathrm{Proj}_{\hat{\boldsymbol{\eta}}_{1\boldsymbol{\omega}}}(\cdot)$ is the discontinuous projection operator, defined as follows.

Definition: $\boldsymbol{\theta} \in \boldsymbol{R}^{\mathrm{P}}$ is the uncertain parameter; $\hat{\boldsymbol{\theta}}$ is the estimation value of $\boldsymbol{\theta}$; and $\tilde{\boldsymbol{\theta}} = \hat{\boldsymbol{\theta}} - \theta$ is the estimation error. $\dot{\hat{\boldsymbol{\theta}}} = \mathrm{Proj}_{\hat{\boldsymbol{\theta}}}(\boldsymbol{\Gamma}\boldsymbol{\tau})$ is the discontinuous-projection adaptive law of $\hat{\boldsymbol{\theta}}$; where $\boldsymbol{\Gamma}$ is a positive diagonal matrix, $\boldsymbol{\tau}$ is an adaptive function; and $\mathrm{Proj}_{\hat{\boldsymbol{\theta}}}(\cdot)$ is the discontinuous projection operator, defined as follows:

$$\mathrm{Proj}_{\hat{\boldsymbol{\theta}}}(\cdot) = \left[\mathrm{Proj}_{\hat{\theta}_1}(*_1), \cdots, \mathrm{Proj}_{\hat{\theta}_p}(*_p)\right]^{\mathrm{T}}$$

$$\mathrm{Proj}_{\hat{\theta}_i}(*_i) = \begin{cases} 0, & \text{if } \hat{\theta}_i = \theta_{i\max} \text{ and } *_i > 0 \\ 0, & \text{if } \hat{\theta}_i = \theta_{i\min} \text{ and } *_i < 0 \\ *_i, & \text{other} \end{cases}$$

The discontinuous-projection adaptive law has the following properties:

Property 1: $\hat{\theta}_i \in [\theta_{i\min}, \theta_{i\max}], i = 1, \cdots, p$

Property 2: $\tilde{\boldsymbol{\theta}}^T\left(\boldsymbol{\Gamma}^{-1}\mathrm{Proj}_{\hat{\boldsymbol{\theta}}}(\boldsymbol{\Gamma}\boldsymbol{\tau}) - \boldsymbol{\tau}\right) \le 0, \forall\boldsymbol{\tau}$

Proof: (1) **Property 1** can be proven from the definition of the discontinuous projection operator.

(2) **Property 2**: If $\hat{\theta}_i = \theta_{i\max}$, we have $\tilde{\theta}_i \ge 0$ and $\mathrm{Proj}_{\hat{\theta}_i}(\boldsymbol{\Gamma}\boldsymbol{\tau})_i = 0$. Because $*_i > 0$, we have $\boldsymbol{\tau} > 0$ and $\tilde{\theta}_i\left(\boldsymbol{\Gamma}^{-1}\mathrm{Proj}_{\hat{\boldsymbol{\theta}}_i}(\boldsymbol{\Gamma}\boldsymbol{\tau})_i - \boldsymbol{\tau}_i\right) \le 0, \forall\boldsymbol{\tau}$. If $\hat{\theta}_i = \theta_{i\min}$, we have $\tilde{\theta}_i \le 0$ and $\mathrm{Proj}_{\hat{\boldsymbol{\theta}}_i}(\boldsymbol{\Gamma}\boldsymbol{\tau})_i = 0$. Since in this case $*_i < 0$, we obtain $\tilde{\theta}_i\left(\boldsymbol{\Gamma}^{-1}\mathrm{Proj}_{\hat{\boldsymbol{\theta}}_i}(\boldsymbol{\Gamma}\boldsymbol{\tau})_i - \boldsymbol{\tau}_i\right) \le 0, \forall\boldsymbol{\tau}$. In addition, when $\mathrm{Proj}_{\hat{\theta}_i}(\boldsymbol{\Gamma}\boldsymbol{\tau})_i = (\boldsymbol{\Gamma}\boldsymbol{\tau})_i$, then $\boldsymbol{\Gamma}^{-1}\mathrm{Proj}_{\hat{\boldsymbol{\theta}}_i}(\boldsymbol{\Gamma}\boldsymbol{\tau})_i - \boldsymbol{\tau}_i = 0$. The proof is complete.

Next, the adaptive disturbance observer is designed as follows for $\hat{\boldsymbol{d}}$ in equation (8).

$$\begin{cases} \hat{\boldsymbol{d}} = \boldsymbol{z} + \boldsymbol{M}(\tilde{\boldsymbol{\omega}}_1) \\ \dot{\boldsymbol{z}} = -\boldsymbol{L}_0(\tilde{\boldsymbol{\omega}}_1)\left[\boldsymbol{z} + \dot{\tilde{\boldsymbol{\omega}}}_1 + \boldsymbol{M}(\tilde{\boldsymbol{\omega}}_1) - \tilde{\boldsymbol{d}}\right] + \hat{\boldsymbol{d}}_1 \\ \dot{\hat{\boldsymbol{d}}}_1 = -\boldsymbol{L}_1(\tilde{\boldsymbol{\omega}}_1)\tilde{\boldsymbol{d}}_1 + \hat{\boldsymbol{d}}_2 \\ \vdots \\ \dot{\hat{\boldsymbol{d}}}_{k-2} = -\boldsymbol{L}_{k-2}(\tilde{\boldsymbol{\omega}}_1)\tilde{\boldsymbol{d}}_{k-2} + \hat{\boldsymbol{d}}_{k-1} \\ \dot{\hat{\boldsymbol{d}}}_{k-1} = -\boldsymbol{L}_{k-1}(\tilde{\boldsymbol{\omega}}_1)\tilde{\boldsymbol{d}}_{k-1}, \end{cases} \tag{10}$$

where k is the degree of the observer; $\boldsymbol{d}_i$ is the i-th differential of $\boldsymbol{d}$, $i = 1, \cdots, k-1$; $\hat{\boldsymbol{d}}_i$ is the estimation value of $\boldsymbol{d}_i$; and $\tilde{\boldsymbol{d}}_i = \hat{\boldsymbol{d}}_i - \boldsymbol{d}_1^i$ is the estimation error. $\boldsymbol{z} \in \mathrm{R}^3$ and $\hat{\boldsymbol{d}}_i \in \mathrm{R}^3$ are the inner states of the observer; $\boldsymbol{M}(\tilde{\boldsymbol{\omega}}_1)$ is the vector-valued function; and $\boldsymbol{L}_i(\tilde{\boldsymbol{\omega}}_1)$ is the gain matrix, with $\boldsymbol{L}_0(\tilde{\boldsymbol{\omega}}_1)$ satisfying the following equation.

$$\boldsymbol{L}_0(\tilde{\boldsymbol{\omega}}_1) = \frac{\partial \boldsymbol{M}(\tilde{\boldsymbol{\omega}}_1)}{\partial(\tilde{\boldsymbol{\omega}}_1)}, \tag{11}$$

The derivative of $\tilde{\boldsymbol{d}}$ can be described as:

$$\begin{aligned} \dot{\tilde{d}} &= \dot{\hat{\boldsymbol{d}}} - \dot{\boldsymbol{d}} = \dot{\boldsymbol{z}} + \frac{\partial \boldsymbol{M}(\tilde{\boldsymbol{\omega}}_1)}{\partial(\tilde{\boldsymbol{\omega}}_1)} \cdot \dot{\tilde{\boldsymbol{\omega}}}_1 - \boldsymbol{d}_1 \\ &= -\boldsymbol{L}_0(\tilde{\boldsymbol{\omega}}_1)\left[\boldsymbol{z} + \dot{\tilde{\boldsymbol{\omega}}}_1 + \boldsymbol{M}(\tilde{\boldsymbol{\omega}}_1) - \tilde{\boldsymbol{d}}\right] \\ &\quad + \hat{\boldsymbol{d}}_1 + \boldsymbol{L}_0(\tilde{\boldsymbol{\omega}}_1) \cdot \dot{\tilde{\boldsymbol{\omega}}}_1 - \boldsymbol{d}_1 \\ &= -\boldsymbol{L}_0(\tilde{\boldsymbol{\omega}}_1)\left[\hat{\boldsymbol{d}} - \tilde{\boldsymbol{d}}\right] + \tilde{\boldsymbol{d}}_1 \\ &= -\boldsymbol{L}_0(\tilde{\boldsymbol{\omega}}_1)\boldsymbol{d} + \tilde{\boldsymbol{d}}_1, \end{aligned} \tag{12}$$

Similarly, we can obtain the derivative of $\tilde{\boldsymbol{d}}_1$ as follows:

$$\begin{aligned} \dot{\tilde{d}}_1 &= \dot{\hat{\boldsymbol{d}}}_1 - \dot{\boldsymbol{d}}_1 \\ &= -\boldsymbol{L}_1(\tilde{\boldsymbol{\omega}}_1)\tilde{\boldsymbol{d}}_1 + \hat{\boldsymbol{d}}_2 - \boldsymbol{d}_2 \\ &= -\boldsymbol{L}_1(\tilde{\boldsymbol{\omega}}_1)\tilde{\boldsymbol{d}}_1 + \tilde{\boldsymbol{d}}_2, \end{aligned} \tag{13}$$

Then, we can obtain the dynamic $\tilde{\boldsymbol{d}}$ as:

$$\begin{cases} \dot{\tilde{d}} = -\boldsymbol{L}_0(\tilde{\boldsymbol{\omega}}_1)\boldsymbol{d} + \tilde{\boldsymbol{d}}_1 \\ \dot{\tilde{\boldsymbol{d}}}_1 = -\boldsymbol{L}_1(\tilde{\boldsymbol{\omega}}_1)\tilde{\boldsymbol{d}}_1 + \tilde{\boldsymbol{d}}_2 \\ \vdots \\ \dot{\tilde{\boldsymbol{d}}}_{k-2} = -\boldsymbol{L}_{k-2}(\tilde{\boldsymbol{\omega}}_1)\tilde{\boldsymbol{d}}_{k-2} + \tilde{\boldsymbol{d}}_{k-1} \\ \dot{\tilde{\boldsymbol{d}}}_{k-1} = -\boldsymbol{L}_{k-1}(\tilde{\boldsymbol{\omega}}_1)\tilde{\boldsymbol{d}}_{k-1} \end{cases}, \tag{14}$$

Let $\tilde{\boldsymbol{d}} = \hat{\boldsymbol{d}} - \boldsymbol{d}$ and $\tilde{\boldsymbol{\eta}}_{1\boldsymbol{\omega}} = \hat{\boldsymbol{\eta}}_{1\boldsymbol{\omega}} - \boldsymbol{\eta}_{1\boldsymbol{\omega}}$; then, $\dot{\tilde{\boldsymbol{\omega}}}_1$ can be described as follows.

$$\dot{\tilde{\boldsymbol{\omega}}}_1 = \boldsymbol{L}_1\tilde{\boldsymbol{\omega}}_1 + \boldsymbol{B}(\boldsymbol{\omega})\tilde{\boldsymbol{\eta}}_{1\boldsymbol{\omega}} + \tilde{\boldsymbol{d}}, \tag{15}$$

Theorem 1: When the TVA with disturbances and parameter uncertainty is fault-free, then $\tilde{\boldsymbol{\omega}}_1$ given by equations (8), (9) and (10) is globally asymptotically stable, i.e., $\lim_{t\to\infty}\tilde{\boldsymbol{\omega}}_1(t) = 0$.

Proof: Consider the following Lyapunov function:

$$V_1(t) = \frac{1}{2}\left(\tilde{\omega}_1^{\mathrm{T}} P_1 \tilde{\omega}_1 + \tilde{\eta}_{1\omega}^{\mathrm{T}} \Gamma_1^{-1} \tilde{\eta}_{1\omega} + \tilde{d}^{\mathrm{T}} \tilde{d}\right) + \frac{1}{2}\left(\tilde{d}_1^{T} \tilde{d}_1 + \cdots + \tilde{d}_{k-1}^{T} \tilde{d}_{k-1}\right), \quad (16)$$

The derivative of $V_1(t)$ can be written as:

$$\begin{aligned}\dot{V}_1(t) = &-\frac{1}{2}\tilde{\omega}_1^{\mathrm{T}} Q_1 \tilde{\omega}_1 + \tilde{\eta}_{1\omega}^{\mathrm{T}} B^{\mathrm{T}}(\omega) P_1 \tilde{\omega}_1 \\ &+ \tilde{\omega}_1^{\mathrm{T}} P_1 \tilde{d} + \tilde{\eta}_{1\omega}^{\mathrm{T}} \Gamma_1^{-1} \dot{\tilde{\eta}}_{1\omega} + \tilde{d}^{\mathrm{T}} \dot{\tilde{d}} \\ &+ \tilde{d}_1^{\mathrm{T}} \dot{\tilde{d}}_1 + \cdots + \tilde{d}_{k-1}^{\mathrm{T}} \dot{\tilde{d}}_{k-1}, \end{aligned} \quad (17)$$

Substituting adaptive laws (9) and equations (14) into (17) using **Property 2** of the discontinuous-projection adaptive law yields the following equation:

$$\begin{aligned}\dot{V}_1(t) \le &-\frac{1}{2}\tilde{\omega}_1^{\mathrm{T}} Q_1 \tilde{\omega}_1 + \tilde{\omega}_1^{\mathrm{T}} P_1 \tilde{d} \\ &+ \left[-L_1^0(\tilde{\omega}_1)\tilde{d}^{\mathrm{T}} d + \tilde{d}^{\mathrm{T}} \tilde{d}_1\right] \\ &+ \left[-L_1^1(\tilde{\omega}_1)\tilde{d}_1^{\mathrm{T}} \tilde{d}_1 + \tilde{d}_1^{\mathrm{T}} \tilde{d}_2\right] \\ &+ \cdots + \left[-\tilde{d}_{k-1}^{\mathrm{T}} L_1^{k-1}(\tilde{\omega}_1)\tilde{d}_{k-1}\right], \end{aligned} \quad (18)$$

The square inequality gives the following equation:

$$\begin{cases} \tilde{\omega}_1^{\mathrm{T}} P_1 \tilde{d} \le \frac{1}{4}\|\tilde{\omega}_1\| + \|P_1\| \left\|\tilde{d}\right\| \\ \tilde{d}^{\mathrm{T}} \tilde{d}_1 \le \frac{1}{4}\left\|\tilde{d}\right\| + \left\|\tilde{d}_1\right\| \\ \vdots \\ \tilde{d}_{k-2}^{\mathrm{T}} \tilde{d}_{k-1} \le \frac{1}{4}\left\|\tilde{d}_{k-2}\right\| + \left\|\tilde{d}_{k-1}\right\|, \end{cases} \quad (19)$$

where $\|*\|$ denotes the matrix norm. Then,

$$\begin{aligned}\dot{V}_1(t) \le &-\frac{1}{2}\tilde{\omega}_1^{\mathrm{T}} Q_1 \tilde{\omega}_1 + \frac{1}{4}\|\tilde{\omega}_1\| + P_{1\max}\left\|\tilde{d}\right\| \\ &+ \left[-L_0(\tilde{\omega}_1)\tilde{d}^{\mathrm{T}} d + \frac{1}{4}\left\|\tilde{d}\right\| + \left\|\tilde{d}_1\right\|\right] \\ &+ \left[-L_1(\tilde{\omega}_1)\left(\tilde{d}_1\right)^{\mathrm{T}} \tilde{d}_1 + \frac{1}{4}\left\|\tilde{d}_1\right\| + \left\|\tilde{d}_2\right\|\right] \\ &+ \cdots + \left[-\tilde{d}_{k-1}^{\mathrm{T}} L_{k-1}(\tilde{\omega}_1)\tilde{d}_{k-1}\right] \\ \le &-\left(\frac{1}{2}Q_{1\min} - \frac{1}{4}\right)\|\tilde{\omega}_1\| \\ &-\left(L_0(\tilde{\omega}_1)_{\min} - P_{1\min} - \frac{1}{4}\right)\left\|\tilde{d}\right\| \\ &-\left(L_1(\tilde{\omega}_1)_{\min} - \frac{1}{4}\right)\left\|\tilde{d}_1\right\| \\ &-\cdots-\left(L_{k-2}(\tilde{\omega}_1)_{\min} - \frac{1}{4}\right)\left\|\tilde{d}_{k-2}\right\| \\ &-L_{k-1}(\tilde{\omega}_1)_{\min}\left\|\tilde{d}_{k-1}\right\|, \end{aligned} \quad (20)$$

where $Q_{1\min}$, $P_{1\min}$ and $L_i(\tilde{\omega}_1)_{\min}$ are the minimum elements of Q_1, P_1 and $L_i(\tilde{\omega}_1)$, respectively. By satisfying equation (20), we achieve $\dot{V}_1(t) \le 0$, meaning that $\tilde{\omega}_1$ given by equations (8), (9) and (10) is globally asymptotically stable, i.e., $\lim_{t\to\infty} \tilde{\omega}_1(t) = 0$, thereby validating the proof.

$$\begin{cases} Q_{1\min} > \frac{1}{2} \\ L_0(\tilde{\omega}_1)_{\min} > P_{1\min} + \frac{1}{4} \\ L_i(\tilde{\omega}_1)_{\min} > \frac{1}{4}, \quad i = 1, \cdots, k-2 \\ L_{k-1}(\tilde{\omega}_1)_{\min} > 0, \end{cases} \quad (21)$$

The fault detection with robustness to disturbances and parameter uncertainty can be designed as follows based on **Theorem 1.**

$$\begin{cases} \|\tilde{\omega}_1\| \le T_1 \rightarrow \text{TVA fault-free} \\ \|\tilde{\omega}_1\| > T_1 \rightarrow \text{TVA fault}, \end{cases} \quad (22)$$

where T_1 is the fault detection threshold.

2) FAULT IDENTIFICATION

For the angle-velocity-loop in equation (4), we design the cascade observer as follows:

$$\dot{\hat{\omega}}_2 = L_2\tilde{\omega}_2 + f(\omega) + B(\omega)\hat{\eta}_{2\omega} + g(\omega)\hat{R}u + \hat{d}, \quad (23)$$

where $\hat{\omega}_2$ is the estimation value of ω and $\tilde{\omega}_2 = \hat{\omega}_2 - \omega$ is the estimation error; L_2 is a solution to the Lyapunov matrix equation $L_2^{\mathrm{T}} P_2 + P_2 L_2 = -Q_2$ with $P_2 = P_2^{\mathrm{T}} > 0$ and $Q_2 = Q_2^{\mathrm{T}} > 0$; and $\hat{\eta}_{2\omega}$ is designed as follows to compensate for parameter uncertainty.

$$\dot{\hat{\eta}}_{2\omega} = \mathrm{Proj}_{\hat{\eta}_{2\omega}}\left\{\Gamma_2\left[-B^{\mathrm{T}}(\omega) P_2 \tilde{\omega}_2\right]\right\}, \quad (24)$$

where Γ_2 is a positive matrix. $\hat{R}$ is the estimation value of R, and $\tilde{R} = \hat{R} - R$ is the estimation error, which is designed as follows to resist the control surface damage.

$$\dot{\hat{R}} = \mathrm{Proj}_{\hat{R}}\left\{-\gamma g^{\mathrm{T}}(\omega) P_2 \tilde{\omega}_2 u\right\}, \quad (25)$$

where $\gamma > 0$. $\hat{d}$ is the estimation value of d, which is designed referring to the observer (10).

$$\dot{\tilde{\omega}}_2 = L_2\tilde{\omega}_2 + B(\omega)\tilde{\eta}_{2\omega} + g(\omega)\tilde{R}u + \tilde{d}, \quad (26)$$

Theorem 2: When the control surface is damaged, then $\tilde{\omega}_2$ given by equations (23)-(25) is globally asymptotically stable, i.e., $\lim_{t\to\infty} \tilde{\omega}_2(t) = 0$.

Proof: Consider the following Lyapunov function:

$$V_2(t) = \frac{1}{2}\left(\tilde{\omega}_2^{\mathrm{T}} P_2 \tilde{\omega}_2 + \tilde{\eta}_{2\omega}^{\mathrm{T}} \Gamma_2^{-1} \tilde{\eta}_{2\omega} + \frac{1}{\gamma}\tilde{R}^{\mathrm{T}}\tilde{R} + \tilde{d}^{T}\tilde{d}\right) + \frac{1}{2}\left(\tilde{d}_1^{T}\tilde{d}_1 + \cdots + \tilde{d}_{k-1}^{T}\tilde{d}_{k-1}\right), \quad (27)$$

The next proof process is similar to **Theorem 1**, and equation (21) makes**Theorem 2**true.

The fault identification can be designed as follows based on **Theorem 1** and**Theorem 2.**

$$\begin{cases} \|\tilde{\omega}_2\| \le T_2 \rightarrow \text{control surface damage} \\ \|\tilde{\omega}_2\| > T_2 \rightarrow \text{actuator fault}, \end{cases} \quad (28)$$

where T_2 is the fault identification threshold.

3) FAULT IDENTIFICATION FOR ACTUATOR FAULTS

To identify actuator faults and estimate the fault parameters, we design two observers based on the adaptation and sliding-mode technique for the ith actuator as follows:

$$\text{Stuck:} \begin{cases} \dot{\delta}_i^s = -a_i\hat{\sigma}_i\left(\delta_i - \delta_{ci}\right) - n_i^s\left(\delta_i^s - \delta_i\right) \\ \hat{\sigma}_i = \text{sgn}\left[a_i\tilde{\delta}_i^s\left(\delta_i - \delta_{ci}\right)\right], \end{cases} \tag{29}$$

$$\text{LOE:} \begin{cases} \dot{\delta}_i^l = -a_i\left(\delta_i - \hat{k}_i\delta_{ci}\right) - n_i^l\left(\delta_i^l - \delta_i\right) \\ \dot{\hat{k}}_i = \text{Proj}_{\hat{k}_i}\left(-a_i\tilde{\delta}_i^l\delta_{ci}\right), \end{cases} \tag{30}$$

where $a_i, n_i^s, n_i^l > 0$, $\tilde{\delta}_i^s = \delta_i^s - \delta_i$, and $\tilde{\delta}_i^l = \delta_i^l - \delta_i$.

Theorem 3: If the ith actuator is stuck, then $\lim_{t\to\infty}\tilde{\delta}_i^s = 0$, $\lim_{t\to\infty}\hat{\sigma}_i = 0$, and $\lim_{t\to\infty}\tilde{\delta}_i^l \neq 0$; if the ith actuator is undergoing LOE, then $\lim_{t\to\infty}\tilde{\delta}_i^s \neq 0$, $\lim_{t\to\infty}\tilde{\delta}_i^l = 0$, and $\lim_{t\to\infty}\tilde{k}_i = 0$, where $\tilde{k}_i = \hat{k}_i - k_i$.

Proof: When the ith actuator is stuck, $\delta_i = 0$, and the stuck observer errors are:

$$\dot{\tilde{\delta}}_i^s = -a_i\hat{\sigma}_i\left(\delta_i - \delta_{ci}\right) - n_i^s\tilde{\delta}_i^s, \tag{31}$$

Consider the following Lyapunov function:

$$V_3(t) = \frac{1}{2}\tilde{\delta}_i^s\tilde{\delta}_i^s, \tag{32}$$

By using the second equation of (29), the derivative of $V_3(t)$ can be described as:

$$\begin{aligned} \dot{V}_3(t) &= \tilde{\delta}_i^s\dot{\tilde{\delta}}_i^s = -n_i^s\left|\tilde{\delta}_i^s\right|^2 - \hat{\sigma}_i a_i\tilde{\delta}_i^s\left(\delta_i - \delta_{ci}\right) \\ &= -\text{sgn}\left(a_i\tilde{\delta}_i^s\left(\delta_i - \delta_{ci}\right)\right)a_i\tilde{\delta}_i^s\left(\delta_i - \delta_{ci}\right) \\ &\quad - n_i^s\left|\tilde{\delta}_i^s\right|^2 \leq 0, \end{aligned} \tag{33}$$

According to Lyapunov stability theory, we have $\lim_{t\to\infty}\tilde{\delta}_i^s = 0$ and $\lim_{t\to\infty}\hat{\sigma}_i = 0$. In addition, the LOE observer error is:

$$\dot{\tilde{\delta}}_i^l = -n_i^l\tilde{\delta}_i^l - a_i\left(\delta_i - \hat{k}_i\delta_{ci}\right), \tag{34}$$

Because $\delta_{ci} \neq 0$ and $\dot{\hat{k}}_i = \text{Proj}_{\hat{k}i}\left[\Psi_i(-a_i\tilde{\delta}_i^l\delta_{ci})\right]$, we can infer that $\dot{\tilde{\delta}}_i^l \neq 0$ and $\lim_{t\to\infty}\tilde{\delta}_i^l \neq 0$.

When the ith actuator is undergoing LOE, then the stuck observer error is:

$$\dot{\tilde{\delta}}_i^s = -n_i^s\tilde{\delta}_i^s - a_i\left[\left(\hat{\sigma}_i - 1\right)\delta_i - \left(\hat{\sigma}_i - k_i\right)\delta_{ci}\right], \tag{35}$$

Because $\hat{\sigma}_i \in \{0, 1\}$ and $\delta_{ci} \neq 0$, we have $\dot{\tilde{\delta}}_i^s \neq 0$ and $\lim_{t\to\infty}\tilde{\delta}_i^s \neq 0$. The LOE observer error is as follows:

$$\dot{\tilde{\delta}}_i^l = -n_i^l\tilde{\delta}_i^l - a_i\left(k_i - \hat{k}_i\right)\delta_{ci}, \tag{36}$$

Consider the following Lyapunov function:

$$V_4(t) = \tilde{\delta}_i^i\tilde{\delta}_i^l + \tilde{k}_i^T\tilde{k}_i, \tag{37}$$

According to **Property 2** of the discontinuous-projection adaptive law, the derivative of $V_4(t)$ can be determined as follows by using the second equation of (30).

$$\begin{aligned} \dot{V}_4(t) &= 2\tilde{\delta}_i^l\dot{\tilde{\delta}}_i^l + 2\tilde{k}_i\dot{\tilde{k}}_i \\ &= -2n_i^l\left|\tilde{\delta}_i^l\right|^2 + 2a_i\tilde{k}_i\delta_{ci}\tilde{\delta}_i^l + 2\tilde{k}_i\dot{\tilde{k}}_i \\ &\leq -n_i^l\left|\tilde{\delta}_i^l\right|^2 \leq 0, \end{aligned} \tag{38}$$

Then, we can obtain $\lim_{t\to\infty}\tilde{\delta}_i^l = 0$ and $\lim_{t\to\infty}\tilde{k}_i = 0$, thereby completing the proof. We set the following performance index to identify an actuator undergoing a stuck fault and an LOE fault according to **Theorem 3**.

$$I_i^j(t) = c_1\left\|\tilde{\delta}_i^j(t)\right\|^2 + c_2\int_{t_0}^{t} e^{-(\tau - t_0)}\left\|\tilde{\delta}_i^j(\tau)\right\|^2 d\tau + c_3\frac{d\left\|\tilde{\delta}_i^j(t)\right\|^2}{dt}, \tag{39}$$

where $j = s, l$ and where c_1, c_2, and c_3 are the weights of proportion, integration and differentiation of $\tilde{\delta}_i^j$, respectively. The type of fault can be identified by the following equation:

$$\begin{cases} I_i^s(t) < I_i^l(t) \rightarrow \text{Stuck} \\ I_i^s(t) > I_i^l(t) \rightarrow \text{LOE}, \end{cases} \tag{40}$$

4) RFDI FLOW DIAGRAM

The flowchart summarizing the aforementioned RFDI process is shown in **Figure 1**.

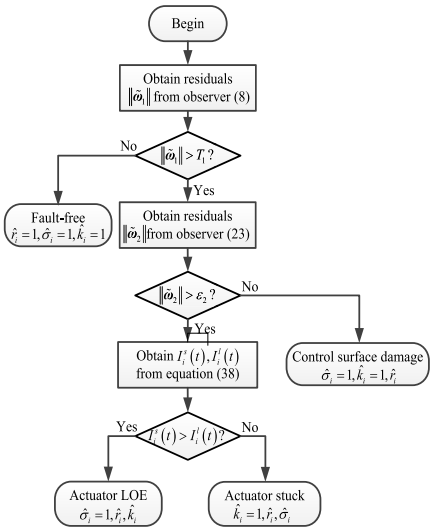

FIGURE 1. Flow diagram of the RFDI mechanism.

B. COMMAND FILTER FTC DESIGN

A command filter [29] FTC system is designed for both the attitude-angle-loop and angle-velocity-loop components that can eliminate the differential expansion in traditional backstepping control [30] by introducing a command filter and accommodating control surface damage, actuator faults,

disturbances and parameter uncertainty by adding the adaptive parameter laws $\hat{\boldsymbol{R}}$, $\hat{\sigma}_i$, $\hat{k}_i$, $\hat{\boldsymbol{d}}$, $\hat{\boldsymbol{\eta}}_{\boldsymbol{\psi}}$ and $\hat{\boldsymbol{\eta}}_{\boldsymbol{\omega}}$ into the command filter backstepping control.

1) ATTITUDE-ANGLE-LOOP CONTROLLER DESIGN

Define the attitude error as

$$\boldsymbol{\psi}_e = \boldsymbol{\psi} - \boldsymbol{\psi}_c, \tag{41}$$

where $\boldsymbol{\psi}_c = [\,\alpha_c \;\; \beta_c \;\; \mu_c\,]^{\mathrm{T}}$ is the command signal. Then,

$$\dot{\boldsymbol{\psi}}_e = \boldsymbol{f}(\boldsymbol{\psi}) + \boldsymbol{A}(\boldsymbol{\psi})\,\boldsymbol{\eta}_{\boldsymbol{\psi}} + \boldsymbol{g}(\boldsymbol{\psi})\,\boldsymbol{\omega} - \dot{\boldsymbol{\psi}}_c, \tag{42}$$

The virtual control signal is designed as follows.

$$\boldsymbol{\omega}_d = \boldsymbol{g}^{-1}(\boldsymbol{\psi})\left[-\boldsymbol{f}(\boldsymbol{\psi}) - \boldsymbol{A}(\boldsymbol{\psi})\,\hat{\boldsymbol{\eta}}_{\boldsymbol{\psi}} - \boldsymbol{K}_{\boldsymbol{\psi}}\boldsymbol{\psi}_e + \dot{\boldsymbol{\psi}}_c\right], \tag{43}$$

where $\boldsymbol{K}_{\boldsymbol{\psi}}$ is a positive matrix and $\hat{\boldsymbol{\eta}}_{\boldsymbol{\psi}}$ is the estimation of $\boldsymbol{\eta}_{\boldsymbol{\psi}}$. Letting $\tilde{\boldsymbol{\eta}}_{\boldsymbol{\psi}} = \hat{\boldsymbol{\eta}}_{\boldsymbol{\psi}} - \boldsymbol{\eta}_{\boldsymbol{\psi}}$, the adaptive law of $\hat{\boldsymbol{\eta}}_{\boldsymbol{\psi}}$ can be designed in the following way:

$$\dot{\hat{\boldsymbol{\eta}}}_{\boldsymbol{\psi}} = \mathrm{Proj}_{\hat{\boldsymbol{\eta}}_{\boldsymbol{\psi}}}\left\{\boldsymbol{\Gamma}_{\boldsymbol{\psi}}\left[\boldsymbol{A}(\boldsymbol{\psi})\,\boldsymbol{\psi}_e - \boldsymbol{\lambda}_{\boldsymbol{\psi}}\tilde{\boldsymbol{\eta}}_{\boldsymbol{\psi}}\right]\right\}, \tag{44}$$

where $\boldsymbol{\Gamma}_{\boldsymbol{\psi}}$ and $\boldsymbol{\lambda}_{\boldsymbol{\psi}}$ are positive matrixes.

Consider the following Lyapunov function:

$$V_5(t) = \frac{1}{2}\left(\boldsymbol{\psi}_e^{\mathrm{T}}\boldsymbol{\psi}_e + \tilde{\boldsymbol{\eta}}_{\boldsymbol{\psi}}^{\mathrm{T}}\boldsymbol{\Gamma}_{\boldsymbol{\psi}}^{-1}\tilde{\boldsymbol{\eta}}_{\boldsymbol{\psi}}\right), \tag{45}$$

By substituting the virtual control signal (42) and the adaptive law (43), the derivative of $V_5(t)$ can be described as:

$$\begin{aligned} V_5(t) &= \boldsymbol{\psi}_e^{\mathrm{T}}\dot{\psi}_e + \tilde{\boldsymbol{\eta}}_{\boldsymbol{\psi}}^{\mathrm{T}}\boldsymbol{\Gamma}_{\boldsymbol{\psi}}^{-1}\dot{\hat{\boldsymbol{\eta}}}_{\boldsymbol{\psi}} \\ &= \boldsymbol{\psi}_e^{\mathrm{T}}\left(\boldsymbol{f}(\boldsymbol{\psi}) + \boldsymbol{A}(\boldsymbol{\psi})\,\boldsymbol{\eta}_{\boldsymbol{\psi}} + \boldsymbol{g}(\boldsymbol{\psi})\,\boldsymbol{\omega} - \dot{\boldsymbol{\psi}}_c\right) \\ &\quad + \tilde{\boldsymbol{\eta}}_{\boldsymbol{\psi}}^{\mathrm{T}}\boldsymbol{\Gamma}_{\boldsymbol{\psi}}^{-1}\mathrm{Proj}_{\hat{\boldsymbol{\eta}}_{\boldsymbol{\psi}}}\left\{\boldsymbol{\Gamma}_{\boldsymbol{\psi}}\left[\boldsymbol{A}(\boldsymbol{\psi})\,\boldsymbol{\psi}_e - \boldsymbol{\lambda}_{\boldsymbol{\psi}}\tilde{\boldsymbol{\eta}}_{\boldsymbol{\psi}}\right]\right\} \\ &\le -\boldsymbol{K}_{\boldsymbol{\psi}}\boldsymbol{\psi}_e^{\mathrm{T}}\boldsymbol{\psi}_e - \boldsymbol{\lambda}_{\boldsymbol{\psi}}\tilde{\boldsymbol{\eta}}_{\boldsymbol{\psi}}^{\mathrm{T}}\tilde{\boldsymbol{\eta}}_{\boldsymbol{\psi}} \le 0, \end{aligned} \tag{46}$$

The attitude-angle-loop controller is thus stable.

2) ANGLE-VELOCITY-LOOP CONTROLLER DESIGN

Based on the adaptive parameter law (25), (29) and (30), the following observer is designed to compensate for actuator faults, control surface damage, disturbances, and parameter uncertainty.

$$\begin{aligned} \dot{\hat{\boldsymbol{\omega}}} = &\boldsymbol{f}(\boldsymbol{\omega}) + \boldsymbol{B}(\boldsymbol{\omega})\,\hat{\boldsymbol{\eta}}_{\boldsymbol{\omega}} + \boldsymbol{g}(\boldsymbol{\omega})\,\hat{\boldsymbol{R}}\hat{\boldsymbol{\Sigma}}\hat{\boldsymbol{K}}u_c \\ &+ \boldsymbol{g}(\boldsymbol{\omega})\,\hat{\boldsymbol{R}}\left(\boldsymbol{I} - \hat{\boldsymbol{\Sigma}}\right)\hat{\boldsymbol{K}}u + \hat{\boldsymbol{d}}, \end{aligned} \tag{47}$$

where $\hat{\boldsymbol{\Sigma}} = diag[\hat{\sigma}_a, \hat{\sigma}_e, \hat{\sigma}_r, \hat{\sigma}_y, \hat{\sigma}_z]$, $\hat{\boldsymbol{K}} = diag[\hat{k}_a, \hat{k}_e, \hat{k}_r, \hat{k}_y, \hat{k}_z]$ and $\hat{\boldsymbol{\eta}}_{\boldsymbol{\omega}}$ is designed as follows to compensate for parameter uncertainty.

$$\dot{\hat{\boldsymbol{\eta}}}_{\boldsymbol{\omega}} = \mathrm{Proj}_{\hat{\boldsymbol{\eta}}_{\boldsymbol{\omega}}}\left\{\boldsymbol{\Gamma}_{\boldsymbol{\omega}}\left[-\boldsymbol{\lambda}_{\boldsymbol{\omega}}\tilde{\boldsymbol{\eta}}_{\boldsymbol{\omega}} - \boldsymbol{B}^{\mathrm{T}}(\boldsymbol{\omega})\,\boldsymbol{\omega}_e\right]\right\}, \tag{48}$$

where $\boldsymbol{\Gamma}_{\boldsymbol{\omega}}$ is a positive matrix and $\boldsymbol{\omega}_e = \hat{\boldsymbol{\omega}} - \boldsymbol{\omega}_d$ is the estimation error. $\hat{\boldsymbol{d}}$, the estimation of $\boldsymbol{d}$, is compensated by an observer, which is designed referring to observer (10).

Take the observer (46) as the auxiliary system; then,

$$\begin{aligned} \dot{\boldsymbol{\omega}}_e = &\boldsymbol{f}(\boldsymbol{\omega}) + \boldsymbol{B}(\boldsymbol{\omega})\,\hat{\boldsymbol{\eta}}_{\boldsymbol{\omega}} + \boldsymbol{g}(\boldsymbol{\omega})\,\hat{\boldsymbol{R}}\hat{\boldsymbol{\Sigma}}\hat{\boldsymbol{K}}u_c \\ &+ \boldsymbol{g}(\boldsymbol{\omega})\,\hat{\boldsymbol{R}}\left(\boldsymbol{I} - \hat{\boldsymbol{\Sigma}}\right)\hat{\boldsymbol{K}}u + \hat{\boldsymbol{d}} - \dot{\boldsymbol{\omega}}_d, \end{aligned} \tag{49}$$

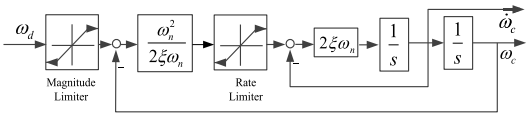

FIGURE 2. Structure of the command filter.

The control law is designed as follows.

$$\begin{aligned} \boldsymbol{u}_c = -&\left[\boldsymbol{g}(\boldsymbol{\omega})\,\hat{R}\hat{\Sigma}\hat{K}\right]^{-1}\left[\boldsymbol{K}_{\boldsymbol{\omega}}\boldsymbol{\omega}_e + \boldsymbol{f}(\boldsymbol{\omega}) + \boldsymbol{B}(\boldsymbol{\omega})\,\hat{\boldsymbol{\eta}}_{\boldsymbol{\omega}}\right. \\ &\left. + \boldsymbol{g}(\boldsymbol{\omega})\left(\boldsymbol{I} - \hat{\boldsymbol{\Sigma}}\right)\hat{\boldsymbol{K}}\hat{\boldsymbol{R}}\boldsymbol{u} + \hat{\boldsymbol{d}} - \dot{\boldsymbol{\omega}}_d\right], \end{aligned} \tag{50}$$

Consider the following Lyapunov function:

$$V_6(t) = \frac{1}{2}\left(\boldsymbol{\omega}_e^T\boldsymbol{\omega}_e + \tilde{\boldsymbol{\eta}}_{\boldsymbol{\omega}}^{\mathrm{T}}\boldsymbol{\Gamma}_{\boldsymbol{\omega}}^{-1}\tilde{\boldsymbol{\eta}}_{\boldsymbol{\omega}} + \boldsymbol{\psi}_e^{\mathrm{T}}\boldsymbol{\psi}_e + \tilde{\boldsymbol{\eta}}_{\boldsymbol{\psi}}^{\mathrm{T}}\boldsymbol{\Gamma}_{\boldsymbol{\psi}}^{-1}\tilde{\boldsymbol{\eta}}_{\boldsymbol{\psi}}\right), \tag{51}$$

By substituting equations (42), (43),, (47) and (48), the derivatives of $V_6(t)$ can be described as follows:

$$\begin{aligned} \dot{V}_6(t) = &-\boldsymbol{K}_{\boldsymbol{\omega}}\boldsymbol{\omega}_e^T\boldsymbol{\omega}_e - \boldsymbol{K}_{\boldsymbol{\psi}}\boldsymbol{\psi}_e^{\mathrm{T}}\boldsymbol{\psi}_e \\ &- \boldsymbol{\lambda}_{\boldsymbol{\psi}}\tilde{\boldsymbol{\eta}}_{\boldsymbol{\psi}}^{\mathrm{T}}\tilde{\boldsymbol{\eta}}_{\boldsymbol{\psi}} - \boldsymbol{\lambda}_{\boldsymbol{\omega}}\tilde{\boldsymbol{\eta}}_{\boldsymbol{\omega}}^{\mathrm{T}}\tilde{\boldsymbol{\eta}}_{\boldsymbol{\omega}} \le 0, \end{aligned} \tag{52}$$

The angle-velocity-loop controller is thus stable.

3) COMMAND FILTER FTC DESIGN

In this section, the command filter is designed to eliminate the impact of the differential expansion belonging to the virtual control ω_d in control law (49). The structure of the command filters is depicted in **Figure 2**.

The state-space model of the command filter is described as

$$\begin{bmatrix}\dot{\boldsymbol{\omega}}_c \\ \ddot{\boldsymbol{\omega}}_c\end{bmatrix} = \begin{bmatrix}\ddot{\boldsymbol{\omega}}_c \\ 2\xi\omega_n\left[S_R\left(\frac{\omega_n^2}{2\xi\omega_n}\left(S_M(\boldsymbol{\omega}_d) - \omega_c\right)\right) - \dot{\boldsymbol{\omega}}_c\right]\end{bmatrix}, \tag{53}$$

where ξ and ω_n are the damping and the bandwidth of the filter, respectively, and $\boldsymbol{\omega}_c$ is the filtered signal of $\boldsymbol{\omega}_d$. $\boldsymbol{\Omega}$ is designed as follows to compensate for the errors of the command filter.

$$\dot{\boldsymbol{\Omega}} = -\boldsymbol{K}_{\boldsymbol{\psi}}\boldsymbol{\Omega} + \boldsymbol{g}(\boldsymbol{\psi})\left(\hat{\boldsymbol{\omega}} - \boldsymbol{\omega}_c\right), \tag{54}$$

Then, the attitude error can be redefined as

$$\bar{\boldsymbol{\psi}}_e = \boldsymbol{\psi}_e - \boldsymbol{\Omega}, \tag{55}$$

The angle velocity error can be redefined as

$$\bar{\boldsymbol{\omega}}_e = \hat{\boldsymbol{\omega}} - \boldsymbol{\omega}_c, \tag{56}$$

The control law is formulated as follows.

$$\boldsymbol{u}_c = -\left[\boldsymbol{g}(\boldsymbol{\omega})\,\hat{\boldsymbol{R}}\hat{\boldsymbol{\Sigma}}\hat{\boldsymbol{K}}\right]^{-1}\begin{bmatrix}\boldsymbol{K}_{\boldsymbol{\omega}}\bar{\boldsymbol{\omega}}_e + \boldsymbol{f}(\boldsymbol{\omega}) \\ +\boldsymbol{B}(\boldsymbol{\omega})\,\hat{\boldsymbol{\eta}}_{\boldsymbol{\omega}} - \boldsymbol{g}(\boldsymbol{\psi})\,\bar{\boldsymbol{\psi}}_e \\ +\boldsymbol{g}(\boldsymbol{\omega})\left(\boldsymbol{I} - \hat{\boldsymbol{\Sigma}}\right)\hat{\boldsymbol{K}}\hat{\boldsymbol{R}}\boldsymbol{u} \\ +\hat{\boldsymbol{d}} - \dot{\boldsymbol{\omega}}_c\end{bmatrix}, \tag{57}$$

Consider the following Lyapunov function:

$$\begin{aligned} V_7(t) = &\frac{1}{2}\left(\bar{\boldsymbol{\omega}}_e^T\bar{\boldsymbol{\omega}}_e + \tilde{\boldsymbol{\eta}}_{\boldsymbol{\omega}}^{\mathrm{T}}\boldsymbol{\Gamma}_{\boldsymbol{\omega}}^{-1}\tilde{\eta}_{\omega}\right) \\ &+ \frac{1}{2}\left(\bar{\boldsymbol{\psi}}_e^{\mathrm{T}}\bar{\boldsymbol{\psi}}_e + \tilde{\boldsymbol{\eta}}_{\boldsymbol{\psi}}^{\mathrm{T}}\boldsymbol{\Gamma}_{\boldsymbol{\psi}}^{-1}\tilde{\eta}_{\psi}\right), \end{aligned} \tag{58}$$

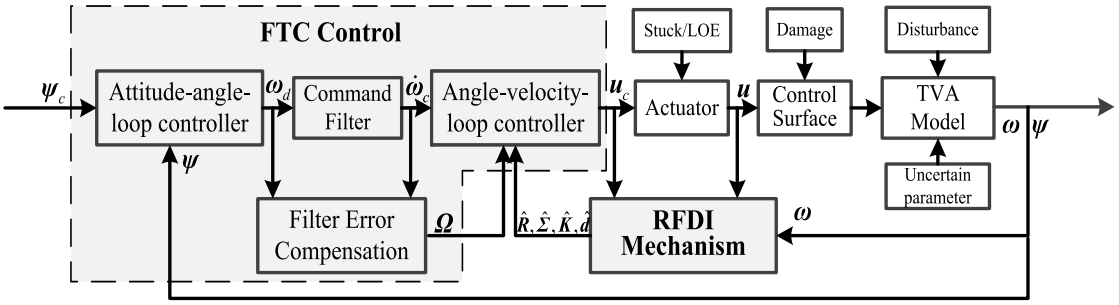

FIGURE 3. The block diagram of the RFDI-FTC system.

By substituting equations (42), (43), (47), (49), (53) and (54), the derivative of $V_7(t)$ can be described as follows:

$$\dot{V}_7(t) = -\boldsymbol{K}_{\omega}\bar{\boldsymbol{\omega}}_e^T\bar{\boldsymbol{\omega}}_e - \boldsymbol{K}_{\psi}\bar{\boldsymbol{\psi}}_e^{\mathrm{T}}\bar{\boldsymbol{\psi}}_e - \boldsymbol{\lambda}_{\psi}\tilde{\boldsymbol{\eta}}_{\psi}^{\mathrm{T}}\tilde{\boldsymbol{\eta}}_{\psi} - \boldsymbol{\lambda}_{\omega}\tilde{\boldsymbol{\eta}}_{\omega}^{\mathrm{T}}\tilde{\boldsymbol{\eta}}_{\omega} \le 0, \quad (59)$$

The command filter FTC is thus stable.

4) STABILITY ANALYSIS FOR THE RFDI-FTC SYSTEM

*Theorem 4:*The RFDI-FTC system for a TVA with control surface damage, actuator faults, disturbances and parameter uncertainty is stable. The system is constituted by the control law (56), the control surface damage parameter law (25), actuator stuck parameter law (29),, actuator LOE parameter law (30), parameter uncertainty law (43) and (47), and the adaptive disturbance observer (10).

Proof: Consider the following Lyapunov function:

$$V_8(t) = \frac{1}{2}\left(\bar{\boldsymbol{\psi}}_e^{\mathrm{T}}\bar{\boldsymbol{\psi}}_e + \tilde{\boldsymbol{\eta}}_{\psi}^{\mathrm{T}}\boldsymbol{\Gamma}_{\psi}^{-1}\tilde{\boldsymbol{\eta}}_{\psi} + \bar{\omega}_e^T\bar{\boldsymbol{\omega}}_e + \tilde{\eta}_{\omega}^{\mathrm{T}}\boldsymbol{\Gamma}_{\omega}^{-1}\tilde{\boldsymbol{\eta}}_{\omega}\right) + \frac{1}{2}\left(\frac{1}{\gamma}\tilde{\boldsymbol{R}}^{\mathrm{T}}\tilde{\boldsymbol{R}} + \sum\tilde{k}_i^2 + \frac{1}{2}\sum\tilde{\sigma}_i^2\right) + \frac{1}{2}\left(\tilde{\boldsymbol{d}}^{\mathrm{T}}\tilde{d} + \tilde{\boldsymbol{d}}_1^T\tilde{\boldsymbol{d}}_1 + \cdots + \tilde{\boldsymbol{d}}_{k-1}^T\tilde{\boldsymbol{d}}_{k-1}\right), \quad (60)$$

The derivative of $V_8(t)$ can be written as:

$$\dot{V}_8(t) = \bar{\boldsymbol{\psi}}_e^{\mathrm{T}}\dot{\bar{\psi}}_e + \tilde{\boldsymbol{\eta}}_{\psi}^{\mathrm{T}}\boldsymbol{\Gamma}_{\psi}^{-1}\dot{\tilde{\boldsymbol{\eta}}}_{\psi} + \bar{\boldsymbol{\omega}}_e^{\mathrm{T}}\dot{\bar{\boldsymbol{\omega}}}_e + \tilde{\boldsymbol{\eta}}_{\omega}^{\mathrm{T}}\boldsymbol{\Gamma}_{\omega}^{-1}\dot{\tilde{\boldsymbol{\eta}}}_{\omega} + \tilde{\boldsymbol{R}}^{\mathrm{T}}\dot{\tilde{R}} + \sum\left(\tilde{k}_i\dot{\tilde{k}}_i + \tilde{\sigma}_i\dot{\tilde{\sigma}}_i\right) + \tilde{\boldsymbol{d}}^T\dot{\tilde{\boldsymbol{d}}} + \cdots + \tilde{\boldsymbol{d}}_{k-1}^T\dot{\tilde{\boldsymbol{d}}}_{k-1}, \quad (61)$$

Substituting adaptive laws (25), (29), (30), (43) and (47) into equation (60) with **Property 2** of the discontinuous-projection adaptive law yields the following equation:

$$\dot{V}_8(t) \le -\boldsymbol{K}_{\psi}\bar{\boldsymbol{\psi}}_e^{\mathrm{T}}\bar{\boldsymbol{\psi}}_e - \boldsymbol{\lambda}_{\psi}\tilde{\boldsymbol{\eta}}_{\psi}^{\mathrm{T}}\tilde{\boldsymbol{\eta}}_{\psi} - \boldsymbol{K}_{\omega}\bar{\boldsymbol{\omega}}_e^T\bar{\boldsymbol{\omega}}_e - \boldsymbol{\lambda}_{\omega}\tilde{\boldsymbol{\eta}}_{\omega}^{\mathrm{T}}\tilde{\boldsymbol{\eta}}_{\omega} - \left(L_0(\bar{\boldsymbol{\omega}}_e)_{\min} - \frac{1}{4}\right)\left\|\tilde{\boldsymbol{d}}_1\right\| - \left(L_1(\bar{\boldsymbol{\omega}}_e)_{\min} - \frac{1}{4}\right)\left\|\tilde{\boldsymbol{d}}_1\right\| - \cdots - \left(L_{k-2}(\bar{\boldsymbol{\omega}}_e)_{\min} - \frac{1}{4}\right)\left\|\tilde{\boldsymbol{d}}_{k-2}\right\| - L_{k-1}(\bar{\boldsymbol{\omega}}_e)_{\min}\left\|\tilde{\boldsymbol{d}}_{k-1}\right\|, \quad (62)$$

TABLE 1. Controller parameters.

parameter	value	parameter	value
Γ_1, Γ_2	diag(2,3,3)	$\boldsymbol{L}_1, \boldsymbol{L}_2$	–diag(3,2,2)
$\boldsymbol{P}_1, \boldsymbol{P}_2$	diag(2,1,3)	$\boldsymbol{Q}_1, \boldsymbol{Q}_2$	diag(12,4,12)
$\boldsymbol{L}_i(\tilde{\boldsymbol{\omega}}_1)$	diag(2,5,4)	k	3
a_i, n_i^s, n_i^l	30,2,3	c_1, c_2, c_3	0.4,0.3,0.3
$\boldsymbol{\Gamma}_{\psi}$	diag(3,8,7)	$\boldsymbol{\lambda}_{\psi}$	diag(8,4,7)
$\boldsymbol{K}_{\psi}$	diag(6,9,4)	$\boldsymbol{K}_{\omega}$	diag(6,7,3)
$\boldsymbol{\Gamma}_{\omega}$	diag(3,2,4, 6,1,3,5,2, 4,5,6,4)	$\boldsymbol{\lambda}_{\omega}$	diag(1,4,7, 3,2,3,2,5, 4,8,6,1)

Letting $L_i(\bar{\boldsymbol{\omega}}_e)_{\min} > 0.25i = 1, \cdots, k-2$ and $L_{k-1}(\bar{\boldsymbol{\omega}}_e)_{\min} > 0$, we obtain $\dot{V}_8(t) \le 0$, meaning that **Theorem 4** is true.

The above description comprises the whole design process of the RFDI-FTC system, whose block diagram is shown in **Figure 3**.

IV. SIMULATION

In this section, the simulation process and results are presented to demonstrate the effectiveness and potential of the proposed RFDI-FTC system.

A. CONTROLLER PARAMETERS

According to the debugging results, we set the controller parameters, as shown in **Table 1**.

B. FAULT SETTING

The simulation lasts 10 s, and we select the parameter uncertainties as $\Delta\boldsymbol{\eta}_{\psi} \in [(1-30\%)\,\boldsymbol{\eta}_{\psi}, (1+30\%)\,\boldsymbol{\eta}_{\psi}]$ and $\Delta\boldsymbol{\eta}_{\omega} \in [(1-20\%)\,\boldsymbol{\eta}_{\omega}, (1+20\%)\,\boldsymbol{\eta}_{\omega}]$ and the external disturbance as $\boldsymbol{d} = [d_p d_q d_r]^T$, where $d_p = d_q = d_r = 10\sin(2\pi t)^{\circ}/s^2$.

In addition, the faults shown in Table 2 arise in the simulation.

TABLE 2. TVA faults in the simulation.

	Time	Fault Type
Condition 1		Fault-free
Condition 2	$t=3$s	Aileron control surface is 80% damaged
	$t=5$s	Elevator control surface is 70% damaged
	$t=7$s	Rudder control surface is 60% damaged
Condition 3	$t=3$s	Elevator actuator is at 70% LOE
	$t=4$s	Aileron control surface is at 70% damage
	$t=5$s	Rudder actuator is at 60% LOE
	$t=6$s	Elevator actuator is stuck
	$t=7$s	Rudder actuator is stuck

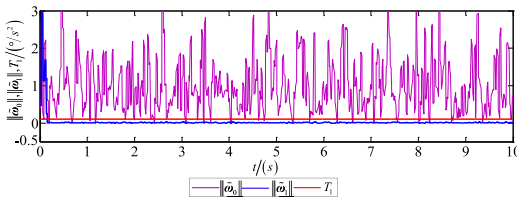

FIGURE 4. The RFDI results of condition 1.

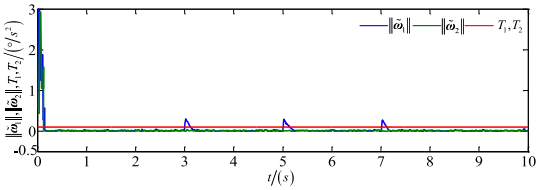

FIGURE 5. The RFDI results of condition 2.

C. SIMULATION RESULTS

Based on the controller parameters and fault setting, the RFDI-FTC simulation results are shown and discussed as follows. The results consist of two parts: the RFDI results to verify the robustness to disturbances and parameter uncertainty in addition to the sensitivity to control surface damage and actuator faults, and the RFDI-FTC results to demonstrate the containment of control surface damage and actuator faults in addition to disturbances and parameter uncertainty.

1) RFDI SIMULATION

The RFDI-FTC simulations, as governed by condition 1, condition 2 and condition 3, are executed, and the RFDI results are shown as follows to demonstrate the system performance. Both T_1 and T_2 are chosen as 0.1.

Condition 1: To present the performance, we compare the simulation results of observer (8) with and without adaptive law (9) and observer (10), whose observer result is called $\tilde{\omega}_0$.

The RFDI results are shown in **Figure 4**. $\|\tilde{\omega}_0\|$ changes irregularly and is greater than T_1 for most of the simulation, causing a false alarm. In contrast, $\|\tilde{\omega}_1\|$ is convergent below T_1 during the whole simulation, showing that no faults occur,

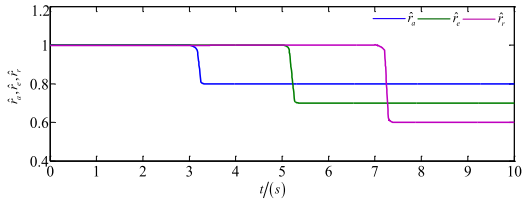

FIGURE 6. The estimation of parameters in condition 2.

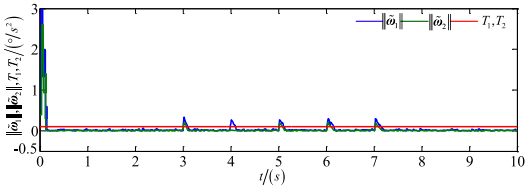

FIGURE 7. The RFDI results of condition 3.

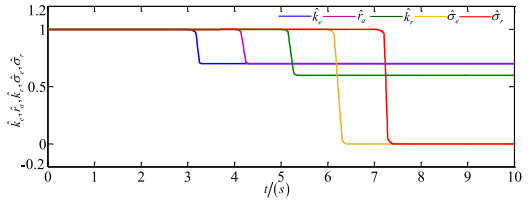

FIGURE 8. The estimation of parameters in condition 2.

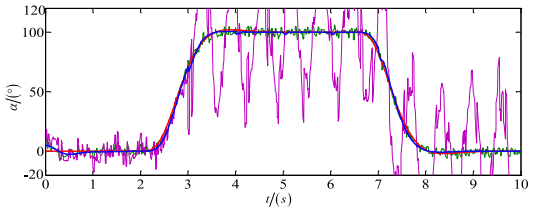

(a) The trace signal of the attack angle

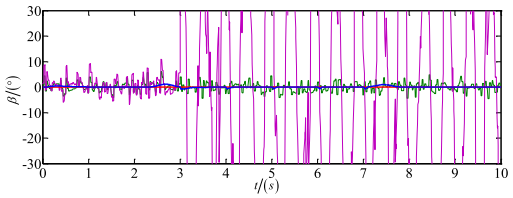

(b) The trace signal of the side-slip angle

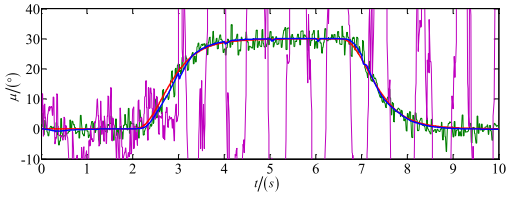

(c) The trace signal of the bank angle

FIGURE 9. The trace signal of the attitude-angle-loop.

which is the same as condition 1 and proves the robustness to disturbances and parameter uncertainty.

Condition 2: The RFDI results of condition 2 are shown in **Figure 5**. $\|\tilde{\omega}_1\|$ is convergent below T_1 during the simulation except at $t=3s$, $t=5s$ and $t=7s$, and $\|\tilde{\omega}_2\|$ is convergent

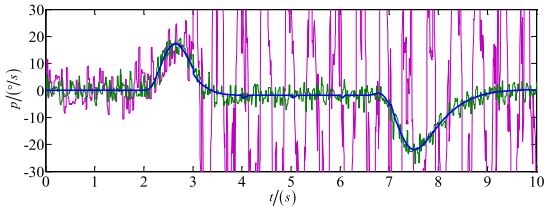

(a) The trace signal of the spin rate

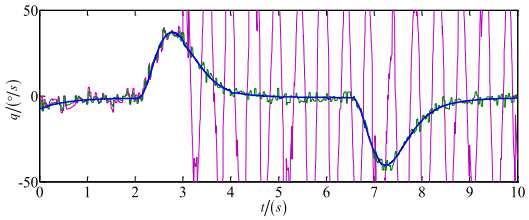

(b) The trace signal of the pitch rate

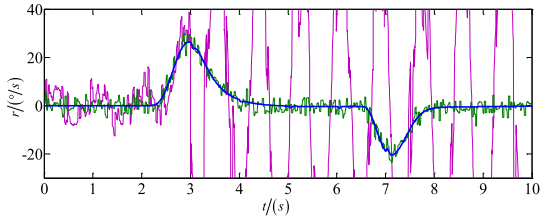

(c) The trace signal of the yaw rate

FIGURE 10. The trace signal of the angle-velocity-loop.

below T_2 during the whole simulation. A comparison of the simulation results between $\|\tilde{\omega}_1\|$ and $\|\tilde{\omega}_2\|$ shows that control surface damage occurs at $t = 3s$, $t = 5s$ and $t = 7s$.

The estimation of parameters in condition 2 is presented in **Figure 6**, which shows that the aileron control surface exhibits 80% damage at $t = 3s$, the elevator control surface exhibits 70% damage at $t = 5s$, and the rudder control surface exhibits 60% damage at $t = 7s$. These results are the same as in condition 2 and prove the sensitivity to control surface damage.

Condition 3: The RFDI results of condition 3 are shown in **Figure 7**. $\|\tilde{\omega}_1\|$ is convergent below T_1 during the simulation except at $t = 3s$, $t = 4s$, $t = 5s$, $t = 6s$ and $t = 7s$, and $\|\tilde{\omega}_2\|$ is convergent below T_2 during the simulation except at $t = 3s$, $t = 5s$, $t = 6s$ and $t = 7s$. A comparison of the simulation results between $\|\tilde{\omega}_1\|$ and $\|\tilde{\omega}_2\|$ reveals control surface damage at $t = 4s$ and actuator faults at $t = 3s$, $t = 5s$, $t = 6s$ and $t = 7s$.

The estimation of parameters in condition 3 is presented in **Figure 8**, which shows that the elevator actuator is at 70% LOE at $t = 3s$, the aileron control surface is at 70% damage at $t = 4s$, the rudder actuator is at 60% LOE at $t = 5s$, the elevator actuator is stuck at $t = 6s$ and the rudder actuator is stuck at $t = 7s$. These results are the same as in condition 3 and prove the sensitivity to actuator faults.

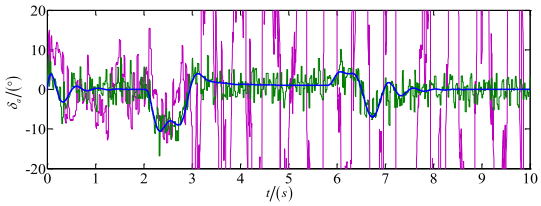

(a) The deflection angle of the aileron actuator

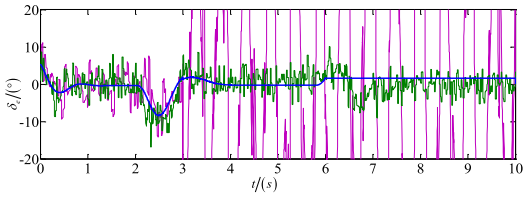

(b) The deflection angle of the elevator actuator

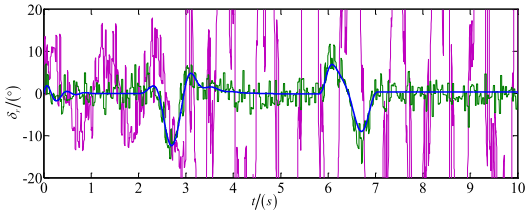

(c) The deflection angle of the rudder actuator

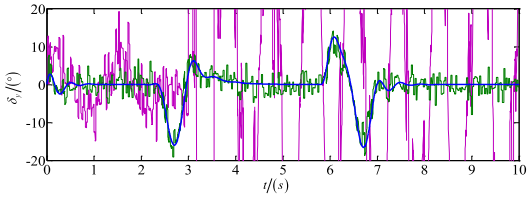

(d) The deflection angle of the lateral thrust-vectoring paddle

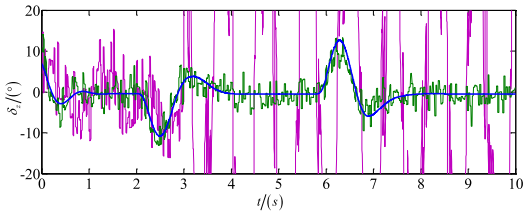

(e) The deflection angle of the longitudinal thrust-vectoring paddle

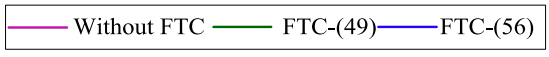

FIGURE 11. The deflection angle of the actuators.

The above simulations comprehensively demonstrate the RFDI system's robustness and sensitivity.

2) RFDI-FTC SIMULATION

The RFDI-FTC simulation is presented to prove its containment of control surface damage and actuator faults and

its robustness to disturbances and parameter uncertainty. To present the performance of the command filter FTC, we compare the simulation results of FTC-(49), FTC-(56) and the absence of FTC, which excludes the control surface damage parameter law (25), actuator stuck parameter law (29), actuator LOE parameter law (30), parameter uncertainty laws (43) and (47), and adaptive disturbance observer (10). The deflection angle limits of δ_a, δ_e, δ_r, δ_y and δ_z are $\pm 15°$, $\pm 15°$, $\pm 15°$, $\pm 20°$, and $\pm 20°$, respectively.

Figure 9 shows the trace signal of the attitude-angle-loop component. We can obtain the following results: the errors without FTC are large from $0 - 3s$ and diverge suddenly because of faults at $t = 3$ s, and FTC-(49) can track the order approximately with irregular fluctuations, whereas the FTC-(56) can track the order both accurately and in a timely fashion. The comparison between FTC-(56) and the absence of FTC demonstrates the containment to control surface damage and actuator faults, as well as robustness to disturbances and parameter uncertainty, and the comparison between FTC-(49) and FTC-(56) presents the superiority of the command filter FTC.

Figure 10 describes the trace signal of the angle-velocity-loop component, and the discussion is similar to that of **Figure 9**.

Figure 11 describes the deflection angle of the actuators. FTC-(56) can ensure that the deflection angles change smoothly within the limits, while the deflection angles without FTC change irregularly and diverge suddenly when faults occur at $t = 3$ s, and the deflection angles in FTC-(49) change irregularly, which proves that FTC-(56) can meet the actual operation requirements more closely than the other approaches. Furthermore, the changes at $t = 3$ s, $t = 5$ s, $t = 6$ s and $t = 7$ s verify that the lateral and longitudinal thrust-vectoring paddle deflections can improve the elevator and rudder deflections, respectively, in TVA during supermaneuverable flight.

The complete simulation results and discussion demonstrate the effectiveness, superiority and potential of the proposed RFDI-FTC system.

V. CONCLUSION

In this paper, a novel RFDI-FTC system for TVA is proposed, and the simulation results imply the following conclusions. (1) The RFDI-FTC system for TVA can detect, identify and accommodate control surface damage and actuator faults under disturbances and parameter uncertainty in the context of highly unsteady and nonlinear flows during supermaneuverable flight. (2) The novel RFDI mechanism based on adaptive observer technology can maintain robustness to disturbances and parameter uncertainty and sensitivity to control surface damage and actuator faults, enhance the accuracy and response speed of FDI, and reduce false alarm rates effectively. (3) The novel command filter FTC based on backstepping can eliminate the impact of differential expansion in traditional backstepping control and compensate for control surface damage, actuator faults, disturbances and parameter uncertainty simultaneously.

In future work, novel observer [31] technology will be studied and incorporated to improve the effectiveness and performance of the RFDI-FTC system for TVA.

REFERENCES

[1] H. X. Zhang, L. Y. Xue, and J. H. Wang, "Research on dynamic control allocation method for aircraft with thrust vector," *Electron. Opt. Control*, vol. 23, no. 12, pp. 71–76, 2016.
[2] L. Kaijun and W. Fawei, "The optimal aiming maneuver control of an aerodynamic/thrust vector control aircraft," in *Proc. IEEE 2nd Inf. Technol., Netw., Electron. Automat. Control Conf. (ITNEC)*, Dec. 2017, pp. 1220–1224.
[3] Y. Li, H. Lu, S. Tian, Z. Jiao, and J.-T. Chen, "Posture control of electromechanical-actuator-based thrust vector system for aircraft engine," *IEEE Trans. Ind. Electron.*, vol. 59, no. 9, pp. 3561–3571, Sep. 2012.
[4] Ö. Atesoglu and M. K. Özgören, "High-alpha flight maneuverability enhancement of a fighter aircraft using thrust-vectoring control," *J. Guid. Control Dyn.*, vol. 30, pp. 1480–1492, 2007.
[5] J. H. Zhu, S. M. Zhang, and C. J. Zhou, "Dynamic characteristics and challenges for control system of super-maneuverable aircraft," *Control Theory Appl.*, vol. 31, no. 12, pp. 1650–1662, 2014.
[6] J. Yang and J. Zhu, "A hybrid NDI control method for the high-alpha super-maneuver flight control," in *Proc. Amer. Control Conf. (ACC)*, Boston, MA, USA, Jul. 2016, pp. 6747–6753.
[7] Ö. Atesoglu and M. K. Özgören, "High-alpha flight maneuverability enhancement of a twin engine fighter-bomber aircraft for air combat superiority using thrust-vectoring control," in *Proc. AIAA Guid., Navigat., Control Conf.*, Jun. 2006, pp. 1–27.
[8] X. Rong, W. Xinmin, and G. Jianying, "Dynamic modeling and simulation for a supermaneuverable aircraft in disturbance of wind field," in *Proc. 5th Int. Conf. Intell. Comput. Technol. Automat.*, Hunan, China, Jan. 2012, pp. 147–150.
[9] S. Hu and J. H. Zhu, "Longitudinal high incidence unsteady aerodynamic modeling for advanced combat aircraft configuration from wind tunnel data," *Sci. China Inf. Sci.*, vol. 60, Nov. 2017, Art. no. 118201.
[10] X. Zhang, F. Zhu, and S. Guo, "Actuator fault detection for uncertain systems based on the combination of the interval observer and asymptotical reduced-order observer," *Int. J. Control*, to be published. doi: 10.1080/00207179.2019.1620329.
[11] H. Jeong, B. Park, S. Park, H. Min, and S. Lee, "Fault detection and identification method using observer-based residuals," *Rel. Eng. Syst. Saf.*, vol. 184, pp. 27–40, Apr. 2018.
[12] N. Moustakis, B. Zhou, T. Le Quang, and S. Baldi, "Fault detection and identification for a class of continuous piecewise affine systems with unknown subsystems and partitions," *Int. J. Adapt. Control Signal Process.*, vol. 32, no. 7, pp. 980–993, Jul. 2018.
[13] X. Zhao, S. Wang, J. Zhang, Z. Fan, and H. Min, "Real-time fault detection method based on belief rule base for aircraft navigation system," *Chin. J. Aeronaut.*, vol. 26, no. 3, pp. 717–729, Jun. 2013.
[14] Z. Gao, Z. Zhou, M. S. Qian, and J. Lin, "Active fault tolerant control scheme for satellite attitude system subject to actuator time-varying faults," *IET Control Theory Appl.*, vol. 12, no. 3, pp. 405–412, Feb. 2018.
[15] Y. Han, S. Oh. B. Choi, D. Kwak, H. J. Kim, and Y. Kim, "Fault detection and identification of aircraft control surface using adaptive observer and input bias estimator," *IET Control Theory Appl.*, vol. 6, no. 10, pp. 1367–1387, Jul. 2012.
[16] X. Wei and M. Verhaegen, "Robust fault detection observer design for linear uncertain systems," *Int. J. Control*, vol. 84, no. 1, pp. 197–215, Feb. 2011.
[17] D. Efimov, J. Cieslak, A. Zolghadri, and D. Henry, "Actuator fault detection in aircraft systems: Oscillatory failure case study," *Annu. Rev. Control*, vol. 37, no. 1, pp. 180–190, Apr. 2013.
[18] A. Nasiri, S. K. Nguang, A. Swain, and D. Almakhles, "Passive actuator fault tolerant control for a class of MIMO nonlinear systems with uncertainties," *Int. J. Control*, vol. 92, no. 3, pp. 693–704, 2019.
[19] S. Ljaz, L. Yan, M. T. Hamayun, and C. Shi, "Active fault tolerant control scheme for aircraft with dissimilar redundant actuation system subject to hydraulic failure," *J. Franklin Inst.*, vol. 356, no. 3, pp. 1302–1332, Feb. 2019.

[20] J. Wang, S. Wang, X. Wang, C. Shi, and M. T. Mileta, "Active fault tolerant control for vertical tail damaged aircraft with dissimilar redundant actuation system," *Chin. J. Aeronaut.*, vol. 29, no. 5, pp. 1313–1325, Oct. 2016.
[21] D. Rajamani and C. Lahouari, "Robust fault-tolerant control using an accurate emulator-based identification technique," *Int. J. Control*, vol. 91, no. 7, pp. 1473–1488, 2018.
[22] Q. Shen, B. Jiang, and V. Cocquempot, "Adaptive fault-tolerant backstepping control against actuator gain faults and its applications to an aircraft longitudinal motion dynamics," *Int. J. Robust Nonlinear Control*, vol. 23, no. 15, pp. 1753–1779, Oct. 2013.
[23] H. Ouyang and Y. Lin, "Supervisory adaptive fault-tolerant control against actuator failures with application to an aircraft," *Int. J. Robust Nonlinear Control*, vol. 28, no. 2, pp. 536–551, Jan. 2018.
[24] A. Chakravarty and C. Mahanta, "Actuator fault-tolerant control (FTC) design with post-fault transient improvement for application to aircraft control," *Int. J. Robust Nonlinear Control*, vol. 26, no. 10, pp. 2049–2074, Jul. 2016.
[25] R. Lamouchi, T. Raïssi, M. Amairi, and M. Aoun, "Interval observer framework for fault-tolerant control of linear parameter-varying systems," *Int. J. Control*, vol. 91, no. 3, pp. 524–533, 2018.
[26] J. D. Boskovic, S. Bergstrom, and R. K. Mehra, "Robust integrated flight control design under failures, damage, and state-dependent disturbances," *J. Guid., Control, Dyn.*, vol. 28, no. 5, pp. 902–917, 2005.
[27] A. B. Brahim, S. Dhahri, F. B. Hmida, and A. Sellami, "Simultaneous actuator and sensor faults reconstruction based on robust sliding mode observer for a class of nonlinear systems," *Int. J. Control Autom. Syst.*, vol. 19, no. 1, pp. 362–371, Jan. 2017.
[28] J. Ma, S. Ni, W. Xie, and W. Dong, "Deep auto-encoder observer multiple-model fast aircraft actuator fault diagnosis algorithm," *Int. J. Control Autom. Syst.*, vol. 15, no. 4, pp. 1641–1650, Aug. 2017.
[29] G. Cui, S. Xu, Q. Ma, Z. Li, and Y. Chu, "Command-filter-based distributed containment control of nonlinear multi-agent systems with actuator failures," *Int. J. Control*, vol. 91, no. 7, pp. 1708–1719, Jul. 2018.
[30] S. Tong, Y. Li, Y. Li, and Y. Liu, "Observer-based adaptive fuzzy backstepping control for a class of stochastic nonlinear strict-feedback systems," *IEEE Trans. Syst., Man, Cybern. B, Cybern.*, vol. 41, no. 6, pp. 1693–1704, Dec. 2011.
[31] J. Zhang, X. Zhao, F. Zhu, and H. Karimi, "Reduced-order observer design for switched descriptor systems with unknown inputs," *IEEE Trans. Autom. Control*, to be published. doi: 10.1109/TAC.2019.2913050.

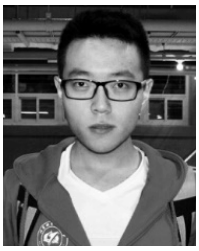

XIAOSHAN MA is currently pursuing the Ph.D. degree in control science and engineering from the Graduate College, Air Force Engineering University, China. His research interests include UAV formation control, fault-tolerant control, and adaptive control.

WENHAN DONG received the Ph.D. degree from the Air Force Engineering University, China, in 2005. He is currently a Professor in navigation, guidance, and control with the Aeronautics and Astronautics Engineering College, Air Force Engineering University. His area of research includes adaptive control and flight control.

BINGQIAN LI is currently a Teaching Assistant from the Aviation Maintenance NCO Academy, Air Force Engineering University. His research interests include UAV formation control and fault-tolerant control.